

Article

Effect of Constraint and Crack Contact Closure on Fatigue Crack Mechanical Behavior of Specimen under Negative Loading Ratio by Finite Element Method

Xinting Miao ^{1,2,*}, Haisheng Hong ¹, Xinyi Hong ¹, Jian Peng ^{1,2} and Fengfeng Bie ^{1,2}¹ School of Mechanical Engineering and Rail Transit, Changzhou University, Changzhou 213164, China² Jiangsu Key Laboratory of Green Process Equipment, Changzhou University, Changzhou 213164, China

* Correspondence: xintingmiao@cczu.edu.cn

Abstract: Mechanical behaviors at fatigue crack tips of cracked specimens under negative loading ratios are studied in detail by the finite element method in this paper. Three factors induced by specimen type and loading type on fatigue crack field are discussed, including constraint, compressive loading effect (CL effect) and crack contact closure. For mode I crack under negative loading ratios, the effects of the CL effect and crack contact closure on plastic strain accumulations are dominant, with the constraint effect being minor. The constraint effect has effects on the monotonous plastic zone, while the CL effect and contact closure both have effects on the reversed plastic zone (RPZ) and residual tensile plastic zone (RTPZ). That is, the higher the constraint, the smaller the size of the monotonous plastic zone; the greater the CL effect, or the smaller the contact degree, the larger the size of RPZ and RTPZ. For mode II crack, there is only CL effect on the crack tip field without the effect of constraint and contact closure, so plastic strain accumulation at the mode II crack tip is much greater than that at the mode I crack tip when they are under the same loading level.



Citation: Miao, X.; Hong, H.; Hong, X.; Peng, J.; Bie, F. Effect of Constraint and Crack Contact Closure on Fatigue Crack Mechanical Behavior of Specimen under Negative Loading Ratio by Finite Element Method.

Metals **2022**, *12*, 1858. <https://doi.org/10.3390/met12111858>

Academic Editor: Alberto Campagnolo

Received: 28 September 2022

Accepted: 27 October 2022

Published: 31 October 2022

Publisher's Note: MDPI stays neutral with regard to jurisdictional claims in published maps and institutional affiliations.



Copyright: © 2022 by the authors. Licensee MDPI, Basel, Switzerland. This article is an open access article distributed under the terms and conditions of the Creative Commons Attribution (CC BY) license (<https://creativecommons.org/licenses/by/4.0/>).

Keywords: over-bend straightening; mold-press straightening; roll-press straightening; prediction model; initial curvature; straightening moment

1. Introduction

1.1. Background

The dynamic load applied to engineering components is often complex in engineering applications. Compressive loading is also a main loading style, which can lead to component failure, except for the common tensile loading style. For example, the fatigue load spectrum applied on aircraft landing gear, submarine and cement structures is mainly compressive loading. Research has validated that the additional reversed plastic damage induced by compressive loading was an important reason for accelerating crack growth [1,2]. If a conservative evaluation criterion is used to evaluate the structural integrity of pressure equipment, with compressive loading in the fatigue loading ignored, it will bring unnecessary losses and disasters.

For cracked specimens under negative loading ratios, crack closure and compressive loading effect are non-negligible factors determining crack growth behaviors [3]. In addition, the constraint is an important factor influencing the fatigue crack tip field, which also must be considered in fatigue crack propagation [4]. There are still shortcomings and contradictions in the research relating to fatigue crack growth behaviors under negative loading ratios; for example, the constraint effect on fatigue crack and test standards of fatigue crack growth under negative loading ratio. So, it is necessary to further study fatigue crack growth behaviors under negative loading ratios, including the constraint effect, the quantification of crack closure and the effect of compressive loading.

1.2. Effects of Constraint on Fatigue Crack Growth

Larsson [5] found that fatigue crack growth behavior was associated with stress state at the crack tip and stress triaxility; that is, specimen type and loading type had effects on fatigue crack growth behavior. Varfolomeev [6] studied fatigue crack growth behaviors by middle tension (MT) specimen, compact tension (CT) specimen, round bar specimen and rectangular specimen with semi-elliptical crack and found that the fatigue crack growth rate of the MT specimen was the fastest, and the fatigue crack growth rate of the CT specimen was the slowest. The main factor is the different stress–strain states in the crack tip vicinity of the specimen caused by specimen type. Fatigue crack growth behaviors of the MT specimen and CT specimen were compared by Hutar [7], who considered that the crack growth rate of the MT specimen was faster than the CT specimen. Ayatollahi [8] has found that specimen type had effects on fatigue crack growth rate and crack growth path. Tong [9] conducted experiments with the CT specimen, SENT specimen and MT specimen and found that the fatigue crack growth rate of the MT specimen was the slowest, while the CT specimen was the fastest, which is opposite to the conclusions of Ayatollahi [7]. Tong also found that the law of fatigue crack growth rate was consistent with that of T -stress. In addition, Zhao [10] found that creep-fatigue behavior was also related to specimen type. Xu [11] has concluded that the fatigue crack growth rate became slower with the loading ratio increasing; the fatigue crack growth rate became faster with the specimen's thickness increasing. The explanation was given in the aspect of crack closure by plastic and three-dimensional constraint.

Fatigue crack growth behaviors of titanium alloy studied by Liknes [12] showed that specimen geometry almost had no effect on the fatigue crack growth rate in the Paris zone. The results indicated that the effect of specimen geometry might be related to material and loading ratio. It was considered the effect of specimen type under a lower stress ratio was greater than that under a higher stress ratio. Deka [13] also studied the constraint effect by changing specimen geometry and loading type on fatigue crack growth. It was concluded that the higher constraint inhibited the accumulation of plastic strain, accompanied by the reduction of the number of triple slip zones near the crack tip. In addition, some other researchers considered the effect of specimen geometry was mainly due to the effect of crack closure.

1.3. Research on Fatigue Crack Growth under Negative Loading Ratio

For a long time, it has been generally believed that fatigue cracks will lead to crack closure and no crack propagation under the action of compressive loading. Moreover, in the standard ASTM E647 [14], only tensile loading in the fatigue cycle was considered, that is, $\Delta K = K_{max}$. At the same time, some research has negated the points. Huang [15] conducted experiments on fatigue crack growth under fatigue compressive loading by MT specimen and double cracked specimen, accompanied by stress–strain field and residual stress analyses by finite element method. It was found that residual tensile stress that occurred during the unloading stage was the main factor influencing fatigue crack growth, whereas compressive loading accelerated crack growth. Pommier [16] found that fatigue crack growth behavior had relationships with both crack tip field ahead of the crack tip and crack contact behavior behind the crack tip. Bian [17] also conducted numerical simulations of the notched specimen and found that fatigue crack growth was associated with the residual stress field after the unloading process. The main driving forces of crack propagation under cyclic compressive loading are the ΔK caused by the alternating change of residual tensile stress field at the crack tip and the reverse compressive stress field caused by the unloading process.

Actually, it is inadequate to demonstrate fatigue crack growth behavior under compressive loading by only residual tensile stress. It must take both the strain field ahead of the crack tip and the plastic wake zone behind the crack tip into consideration [3]. Zhang [18] also proved that the effect of crack closure and compressive loading varied during the fatigue crack growth process. In the previous stage, the crack closure effect was dominant

when the crack growth rate was slower, while in the later stage, the compressive loading effect was dominant when the crack growth was faster.

Therefore, in order to figure out the mechanism of fatigue crack growth of specimen under negative loading ratio, several factors on fatigue crack tip mechanical behaviors, including constraint, compressive loading effect and crack closure effect, are discussed by finite element method in this paper.

2. Finite Element Model and Verification

2.1. Research Scheme

The shapes and sizes of specimens studied in this paper are shown in Figure 1. The width is $W = 20$ mm, the thickness is $B = 10$ mm and the crack length a is equal to the sum of the notch length a_n and the crack length a_s , which is 10 mm. In the fatigue crack growth standard [14,19], the notch length a_n is suggested between $0.1 W$ and $0.15 W$ or $0.2 W$ and the length of pre-crack is also required. However, the influence of the contact between crack surfaces under negative loading cannot be ignored [20]; that is, the notch length a_n of the specimen has an influence on the test results. Therefore, this paper will study the influence of contact degree on the mechanical behavior of fatigue crack tip by changing the notch length a_n (Figure 1). In addition, constraint at the crack tip is the behavior that prevents the plastic from deforming [4], and the influence on the fatigue crack tip field also exists [6–9]. In this paper, different constraints are obtained by changing the position of the loading point (K1 and K3 in Figure 1). The purpose of this paper is to provide a reference for the standardization of fatigue fracture research under negative loading.

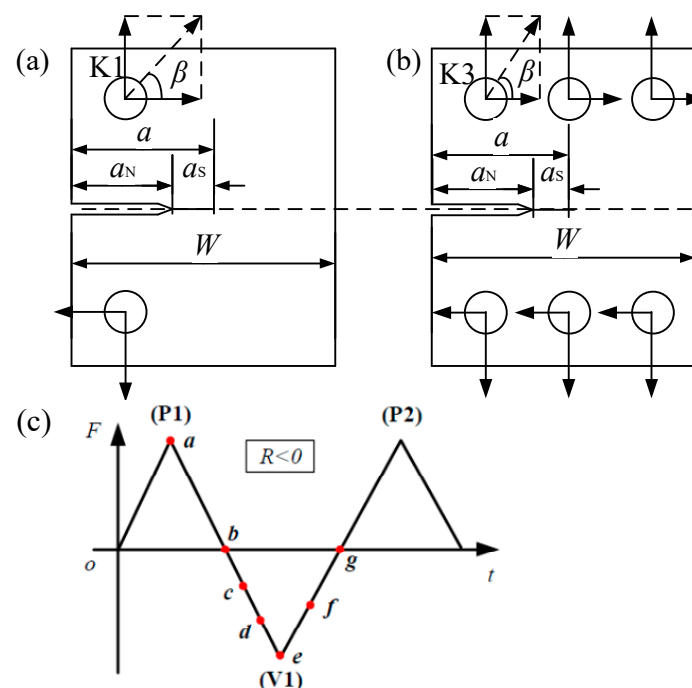


Figure 1. Sketch map of specimen and loading: (a) K1 specimen, (b) K3 specimen, (c) fatigue loading.

Two notch lengths are considered in this paper: $a_n = 0$ and $a_n/a_s = 4$. The specimen with $a_n = 0$ is represented by K-S, and the specimen with $a_n/a_s = 4$ is represented by K-N. Two different loading conditions are considered in this paper, as shown in Figure 1. There are: The loading points are located on both sides of the crack surfaces in Figure 1a, which shows a high constraint state; The loading points are uniformly distributed over the width of the specimen in Figure 1b, which shows a low constraint state.

In Figure 1, the load perpendicular to the crack surface causes the crack opening deformation; the crack tip presents the mode I state. The load parallel to the crack causes

the crack shearing deformation; the crack tip presents the mode II state. I–II mixed mode crack can be obtained by changing loading angle β in Figure 1. Three loading angles of $\beta = 0^\circ$, $\beta = 60^\circ$ and $\beta = 90^\circ$ are considered to study mode I crack, mode II and I–II mixed mode crack in this paper, among which $\beta = 90^\circ$ corresponds to mode I crack, $\beta = 0^\circ$ corresponding to mode II crack, and $\beta = 60^\circ$ corresponding to I–II mixed mode crack. The first four subsections of this paper mainly discuss mode I crack, and the final subsection mainly discusses I–II mixed mode crack.

At the same time, in order to study the influence of negative loading ratio on the mechanical behavior of fatigue crack tip, six negative loading ratios R are considered in this paper, which is shown in Table 1. J -integrals of all specimens at first peak loading points are consistent, which are $1.4 J/N$. The load diagram is shown in Figure 1c. Specimens involved in the text are summarized in Table 1, and the corresponding specimen labels are K1-N, K1-S, K3-N and K3-S.

Table 1. Summary of specimen type and loading type.

Specimen	Loading Point Ki	Contact Type	Loading Angle $\beta/^\circ$	Loading Ratio R
K1-N	K1	N	90	0, -0.1, -0.5, -1, -1.5, -2
K1-S	K1	S	90	0, -0.1, -0.5, -1, -1.5, -2
K3-N	K3	N	90, 60, 0	0, -0.1, -0.5, -1, -1.5, -2
K3-S	K3	S	90	0, -0.1, -0.5, -1, -1.5, -2

2.2. Finite Element Model

In this chapter, the commercial software ABAQUS is used for finite element analyses. Crack surfaces will appear local or even completely closed in the unloading stage when specimens are under negative loadings. Therefore, material nonlinearity (plastic deformation) and geometric nonlinearity (crack surface contact) of the finite element model should be considered simultaneously in the modeling [4,21]. In addition, the effect of the cyclic plastic behavior of material on fatigue crack growth must be considered for cracked specimens under compressive fatigue loading. In this paper, the Chaboche model [22] is used to simulate the cyclic plastic behavior of the material, which can describe the nonlinear mechanical behavior of materials combined with follow-up strengthening and isotropic strengthening. The material studied in this paper is commercially pure titanium TA2. The material characteristic parameters of its Chaboche model have been obtained in reference [21].

The finite element model based on ABAQUS software is shown in Figure 2. One end of the specimen is fixed (F), and one end is applied with fatigue loading (L). The loading fixture adopts a rigid body, and special contacts are set between the fixture and specimen to transfer loading. Special contacts are also set between crack surfaces to prevent the crack surface grids from penetrating each other under the action of compressive load. The continuous 4-node plane strain reduction integral element (CPE4R) is used in the whole model. It is found that the results of finite element simulation are independent of the mesh size when the mesh size at the crack tip is less than 0.05 mm [21]. In order to study mechanical behaviors within the small range around the crack tip, mesh sizes around the crack tip within 20 μm are 1 μm .

2.3. Mesh Verification

Fatigue crack can be closed (even for a part of the tensile phase) as a result of the closing of its lips near the tip under compressive loading. This phenomenon is known as crack closure [23], which has many effects on fatigue crack growth. Special contact has been defined between crack surfaces in this paper in order to demonstrate the accuracy of the contact setting, crack opening displacement (COD) at the crack wake area, and equivalent plastic strain (EPS) ahead of the crack tip was discussed here. CODs at 10th valley points with loading ratios R are shown in Figure 3a,b (D is the distance from the crack tip at the crack wake area), which decrease with R and most of which are less than 0. It is due to

the error in FEM simulation causing intersects between crack surfaces. However, the error of COD is acceptable (the minimum CODs are less than -0.01 mm) and has no effect on fatigue mechanical behavior.

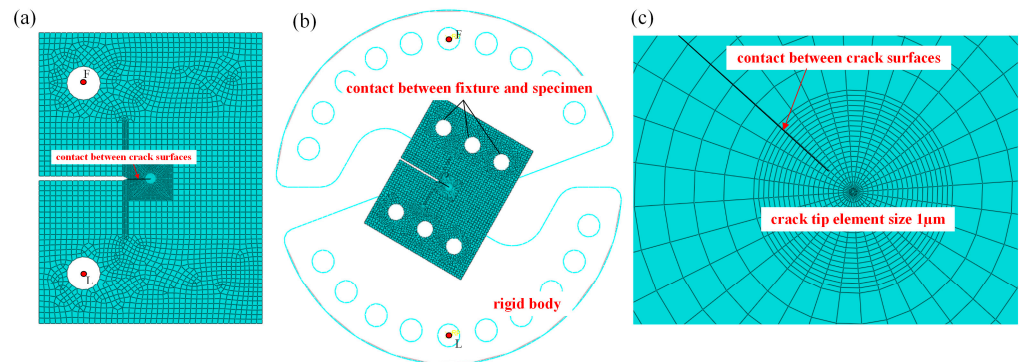


Figure 2. Finite element model: (a) mode I crack, (b) I-II mixed mode crack, (c) mesh detail.

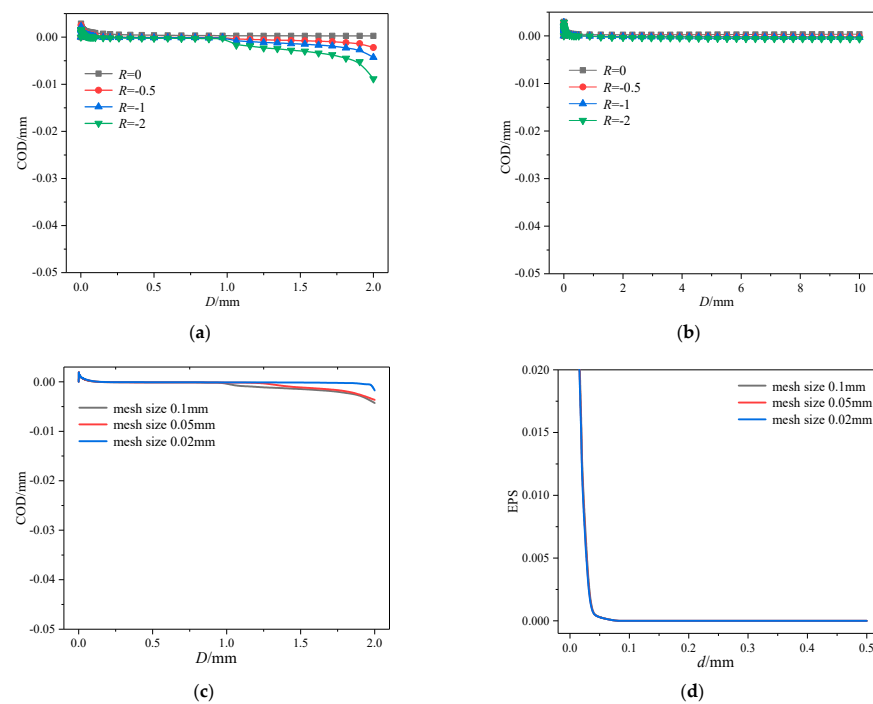


Figure 3. Researches of contact between crack surfaces: (a) effect of R on COD for K3-N, (b) effect of R on COD for K1-S, (c) effect of mesh size on COD ($R = -1$), (d) effect of mesh size on EPS ($R = -1$).

The factors influencing CODs between crack surfaces are the contact coefficient set in ABAQUS and mesh size at the crack surface area. Through computing, the contact coefficient has no effect on vertical contact behavior, while mesh size has an effect. The effects of mesh size are shown in Figure 3c; it can be found that the smaller the mesh size, the lighter the intersection degree between crack surfaces. Plastic strain accumulation ahead of the crack tip is a significant factor relevant to fatigue crack growth behavior, so EPS ahead of the crack tip at the 10th valley point of K3-N specimens is studied in Figure 3d (d is the distance from the crack tip ahead of the crack tip). It can be found that although CODs are affected at the crack wake area, EPS ahead of crack tips almost remains the same. It is mainly due to CODs or intersections between crack surfaces being minor, which will not change the mechanical behavior ahead of the crack tip. So, mesh sizes of contact surfaces in the models are set as 0.1 mm, which gives consideration to both simulating accuracy of mechanical behavior and calculating speed in the computer.

Moreover, contacting stresses (per Newton) between crack surfaces are shown in Figure 4. From the figure, contact stress increases with the loading ratio decreasing. The maximum contact stresses of K3-N, K1-N and K3-S are in the range of 1~2 mm away from crack tips, while the maximum contact stress of K1-S is at the end of the crack. The above phenomena indicate that crack surfaces contact each other with compressive loading applied, and the contact degree is related to contact stress, which also verifies the accuracy of models in this paper.

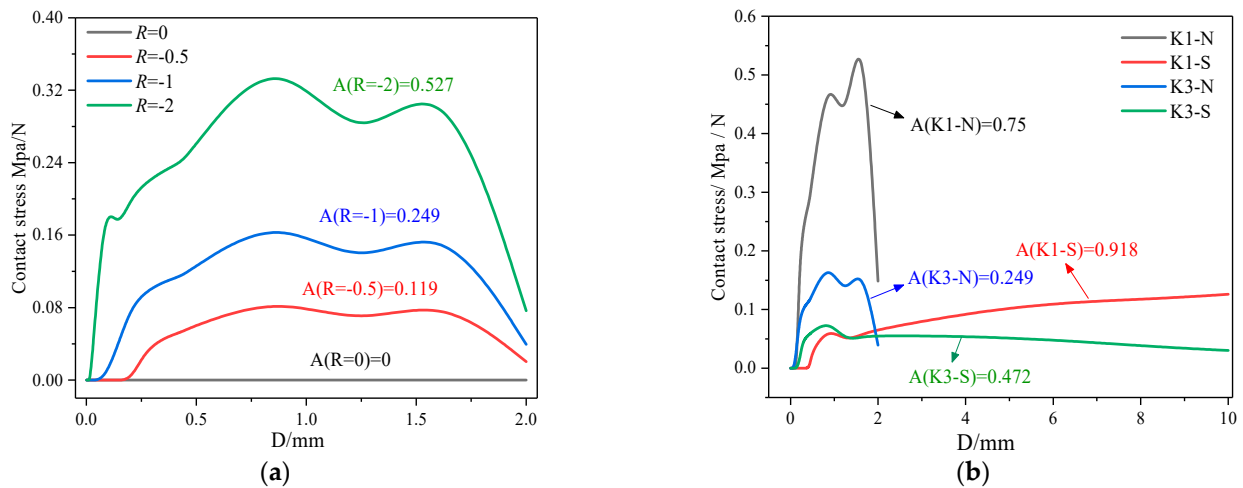


Figure 4. Research of contact stress: (a) effect of loading ratio, (b) effect of specimen type.

3. Quantification of Constraint, Compressive Loading and Contact Closure

3.1. Constraint Ahead of Crack Tip

In order to discuss the effect of constraint, compressive loading and crack closure caused by crack surfaces contact under a negative loading ratio, parameters quantifying the constraint, compressive loading and contact degree are provided in this section.

For specimens in Table 1, the stress fields at the maximum tensile loading level of $J = 1.4 \text{ N/mm}$ are provided in Figure 5. From the figure, it can be found that σ_{yy} of all the specimens are the same, while σ_{xx} are related to loading type, with notch length no effect. The differences between σ_{xx} stress fields can be described by the constraint parameter T-stress. The dimensionless parameter B ($B = \frac{T\sqrt{\pi a}}{\sqrt{k_I^2 + k_{II}^2}}$) [24] is used in this paper; the values of B for K1 specimens are 0.45 and for K3 specimens are 0.23. So, the constraint of the K1 specimen is higher than that of the K3 specimen.

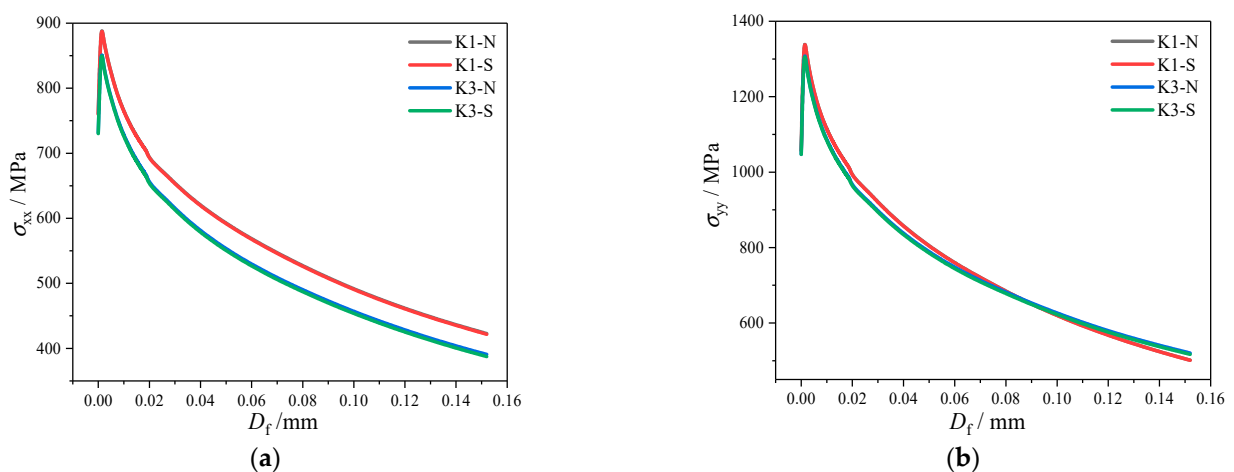


Figure 5. Stress distribution under tensile loading: (a) σ_{xx} ; (b) σ_{yy} .

3.2. Compressive Loading Effect (CL Effect)

Negative stresses ahead of crack tips will occur when specimens are under compressive loadings. Stress components σ_{yy} with distance d are shown in Figure 6 in order to discuss the compressive loading effect, which are stresses at 1st valley points (σ_{yy} at 1st peak point are the same due to the same J -integral at the crack tip). The greater the negative stresses, the more obvious the compressive loading effect, and the greater the plastic damage at the crack tip, which will be discussed in the following paper. The compressive loading effect is abbreviated as the CL effect, so from the figure, it can be obtained as follows: the smaller the loading ratio R , the greater the effect of CL, and $CL(K3-N) > CL(K3-S) > CL(K1-N) > CL(K1-S)$.

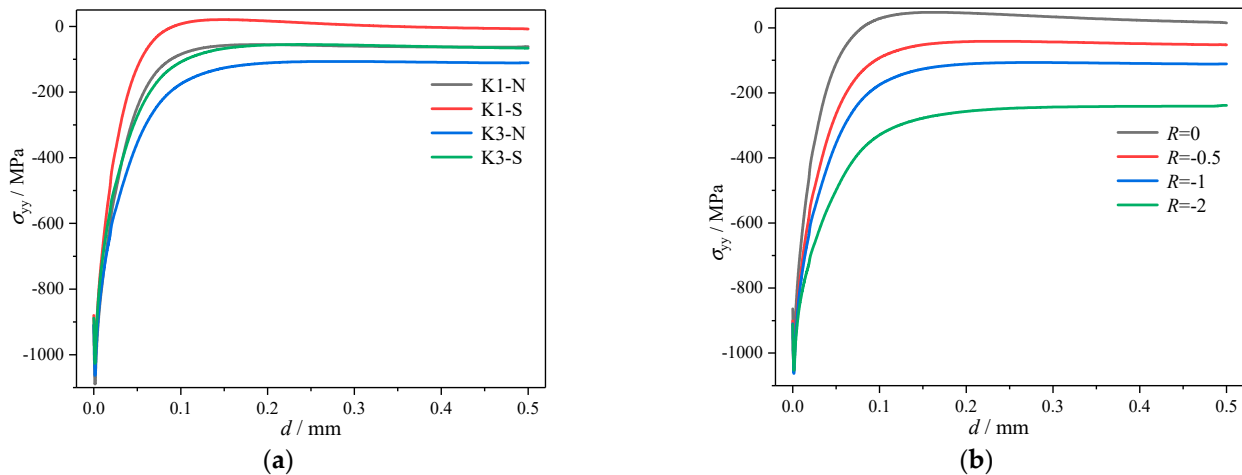


Figure 6. Normal stresses σ_{yy} with d : (a) effect of specimen type, (b) effect of loading ratio.

3.3. Contact Degree at Crack Tip Wake Zone

Crack surfaces will contact specimens under fatigue loadings with negative loading ratios, and the effect of contact degree on fatigue crack tip field cannot be ignored. Contact degree can be quantified by contact stress between crack surfaces, by which the contact coefficient is defined. The contact coefficient C is defined as the contact force under negative loading per Newton, which is expressed as $C(i) = S(i)/A$, among the equation $S(i)$ means contact stress at any point in the crack wake area per newton, A is the area enclosed by contact stress curves in Figure 4 meaning the sum of contact stress along crack wake.

The point of maximum stress shown in Figure 4 means the greatest contact degree, where the regulation of contact coefficient C with loading time is shown in Figure 7. In the figure, the value of C keeps zero when crack surfaces are not closed (before the crack contact point); the value of C becomes greater with contact faces gradually closed until C reaches the maximum at the valley point (recovery point); then the value of C decreases with contact faces gradually separated and contact stress becomes smaller, C keeps zero (recovery end point) again until crack surfaces are separated completely. During the loading–unloading process, crack surfaces keep closed between the process crack contact point and recovery end point, which is the crack closure process.

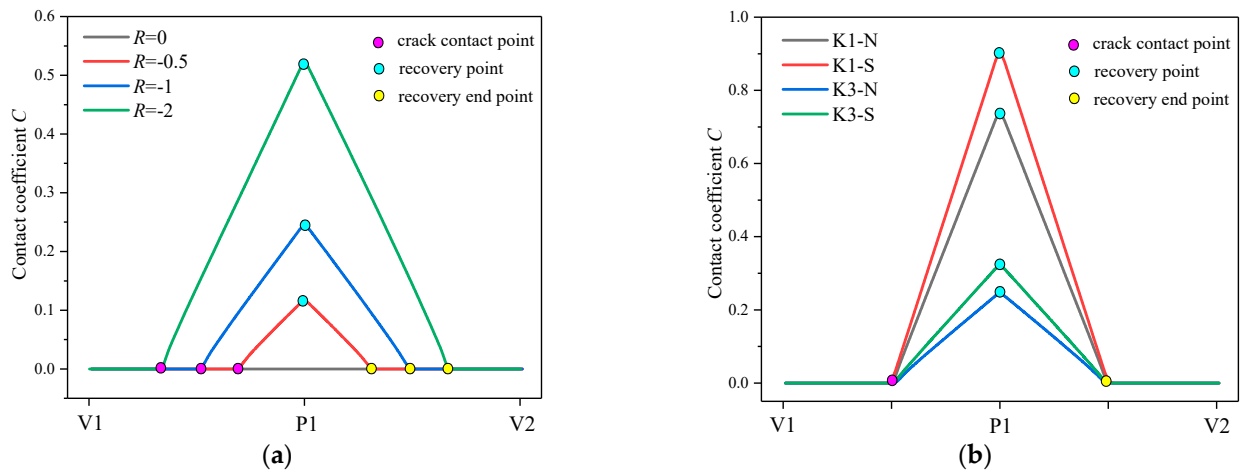


Figure 7. Regulations of contact coefficients C : (a) effect of loading ratio R , (b) effect of specimen type.

The contact coefficient C proposed in the paper is the quantification of contact degree; that is, the greater the value of C , the higher the contact degree, the higher degree of crack contact closure, and the higher the resistance of plastic strain at the crack tip. The relations between contact coefficients C of specimens under different loading ratios are: $C(R = -2) > C(R = -1) > C(R = -0.5) > C(R = 0)$; The relations of contact coefficients C for different types of specimens are: $C(K1-S) > C(K1-N) > C(K3-S) > C(K3-N)$.

The following paper will discuss the mechanical behaviors at fatigue crack tips through three factors of constraint B , compressive loading effect CL , and contact degree C .

4. Study of Stress–Strain Field Ahead of Crack Tip

4.1. Strain Field Ahead of Crack Tip

4.1.1. Circumferential Distribution of Equivalent Plastic Strain (EPS)

Equivalent plastic strain (EPS) is a measure of plastic deformation of the material, which is a scalar. The physical meaning of EPS is to record the deformation history of material and to characterize the cumulative value of plastic strain. The effects of loading ratio and specimen type on circumferential EPS distributions are shown in Figure 8a,b, respectively; the circumferential path studied is $1 \mu\text{m}$ away from the crack tip at the 10th cycle. In the figures, 0° corresponds to the crack tip zone, along which the crack grows, and 180° corresponds to the crack tip wake zone; the solid line corresponds to the EPS field at the peak loading point, the dashed line corresponds to the EPS field at valley loading point; the area enclosed between them is the accumulated plastic strain ahead of crack tip increased by one unloading.

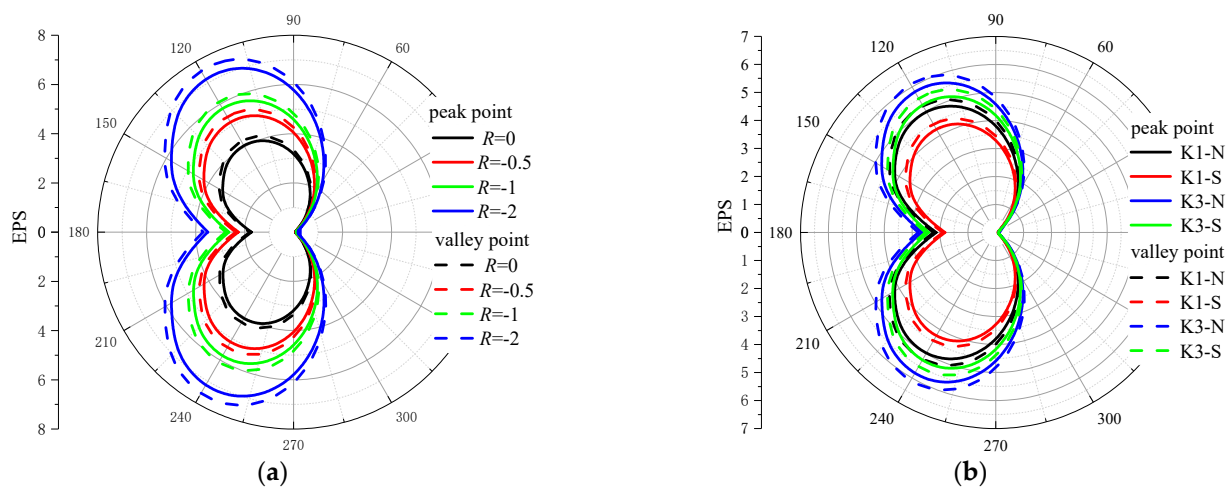


Figure 8. Circumferential distribution of EPS: (a) effect of loading ratio R , (b) effect of specimen type.

The higher the plastic strain accumulation, the greater the damage at the crack tip, and the more likely the specimen is to fail. From Figure 8a, plastic strain accumulation increases as the loading ratio decreases, which means that the negative loading promotes plastic strain accumulation at the crack tip. From Figure 8b, EPS regulations for different types of specimens are consistent with those of CL effect and contrary to those of contact coefficient C ; that is, $EPS(K3-N) > EPS(K3-S) > EPS(K1-N) > EPS(K1-S)$. Associated with the CL effect and contact coefficient C , it can be concluded that the higher the CL effect, or the lower the contact degree, the more damage accumulation ahead of the crack tip.

4.1.2. Effect of Loading Ratio R on Strain Evolution with Loading History

Crack surfaces will contact each other for specimens under compressive loadings, by which the crack tip state will be affected. Strain evolutions are discussed to point out the contact effect during the loading–unloading process. The distributions of strain (E_{yy}) and EPS of the points $2\ \mu\text{m}$ away from crack tips with loading histories for K3-N specimens are shown in Figure 9.

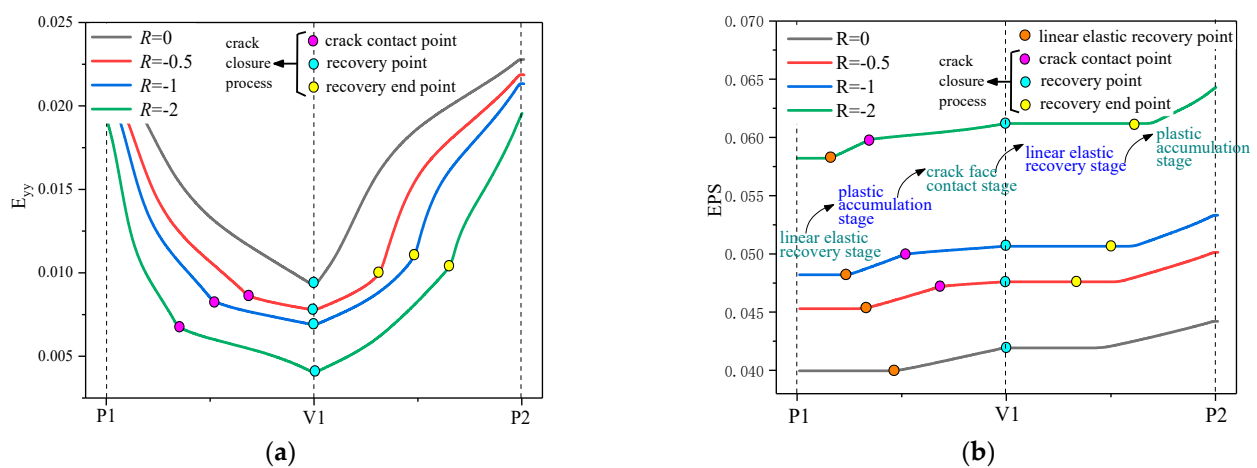


Figure 9. Effect of loading ratio on strain field: (a) E_{yy} with loading history for K3-N, (b) EPS with loading history for K3-N.

As shown in Figure 9a, strain (E_{yy}) decreases and then increases, but the decreasing/increasing rate is not constant. Especially for the crack contact point and recovery end point, the decreasing/increasing rate of strain(E_{yy}) incites a sudden decrease/increase due to crack surfaces contacting (crack contact point)/separating (recovery end point) with

each other. The phenomenon is called crack contact closure, and the process between the crack contact point and recovery end point is the crack closure process. Correspondingly, the increasing/decreasing rate of EPS in Figure 9b decreases/increases due to crack surfaces contacting/separating with each other. The history of EPS can be divided into five stages, including the linear-elastic recovery stage (unloading), plastic accumulation stage (unloading), crack face contact stage, linear-elastic recovery stage (loading) and plastic accumulation stage (loading); the recovery end point is in the linear-elastic recovery stage (loading).

From the figures, the crack closure process related to crack contacting closure becomes larger with the loading ratio decreasing. Combined with the contact coefficient C and CL effect, it can be concluded that the smaller the loading ratio R , the greater the contact coefficient C , the smaller the CL effect, the larger the crack closure process and the greater the hinder effect on plastic strain accumulation. At the same time, the CL effect is much greater than that of the crack contact closure effect during the loading–unloading process. So, negative loading promotes plastic strain accumulation at the crack tip, and EPS at the crack tip increases with loading ratio R , which is mainly induced by the CL effect.

4.1.3. Effect of Specimen Type on Strain Evolution with Loading History

Figure 10 shows EPS of the point 2 μm away from crack tips with loading histories for specimens under $R = 0$ and -1 , respectively; the aim is to discuss the effect of constraint, CL effect and crack contact closure on fatigue crack growth.

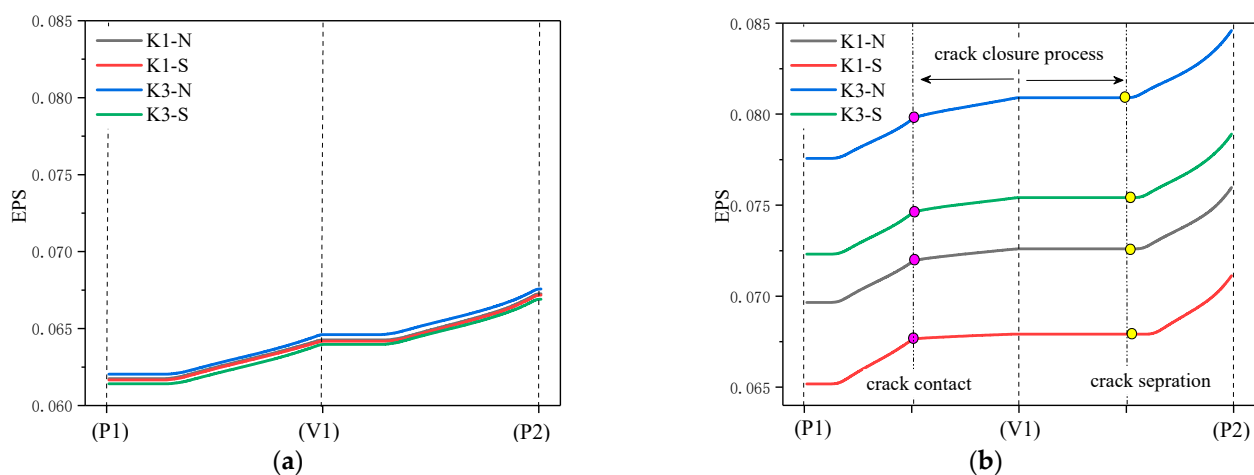


Figure 10. Effect of specimen type on EPS distribution: (a) $R = 0$, (b) $R = -1$.

Conclusions have been drawn from Figures 3 and 4, that is $B(K1) > B(K3)$, $CL(K1) < CL(K3)$, $C(Ki-S) > C(Ki-N)$ ($i = 1, 3$), based on which strain evolution is discussed. Firstly, the effect of constraint (Figure 10a) is: the higher the constraint (K1 specimen), the lower the EPS, or the lower the plastic strain accumulation; it is mainly because the higher the constraint, the greater the resistance to plastic deformation at the crack tip during the loading process. The CL effect (Figure 10b) is: the greater the CL effect (K3), the greater the EPS. Then, the effect of crack contact closure (Figure 10b) is: the greater the crack contact closure C (Ki-S specimen), the lower EPS at the crack tip; this is because the greater the contact degree C , the higher the closure degree at the crack tip, the greater the resistance to plastic strain at the crack tip. Zhang [21] also proved that crack contacting closure reduced the cumulative rate of EPS through tests and finite element methods, but the impact of contact degree has not been discussed.

The differences in EPS of different specimens under $R = 0$ are smaller in Figure 10a, which is mainly caused by constraint, while differences in EPS of different specimens under $R < 0$ are larger, which is related to the CL effect and crack contact closure. So, (1) For specimens under fatigue loadings with $R \geq 0$, the differences of plastic strain accumulations are mainly induced by constraint, whose effects are smaller, relatively; and the effect of

crack closure is also smaller. (2) Among these specimens, the EPS of the K3-N specimen is maximum, and the EPS of the K1-S specimen is minimum, which is consistent with the laws of CL effects and contact degrees C ; that is, the greater the CL effect or the smaller the C , the greater the EPS.

4.2. Stress Field Ahead of Crack Tip

4.2.1. Circumferential Mises Stress Distribution

Circumferential Mises stress distributions at the paths 2 μm away from crack tips are shown in Figure 11. At valley loading in Figure 11b, Mises stresses of most areas increase with loading ratio R decreasing, including crack tip wake zone; this is due to contacting behavior between crack surfaces. While at peak loading in Figure 11a, Mises stress decreases as loading ratio R decreases at the crack tip wake zone, which is opposite to that in other areas around the crack tip; this is mainly because stress at peak loading is offset by compressive stress at valley loading.

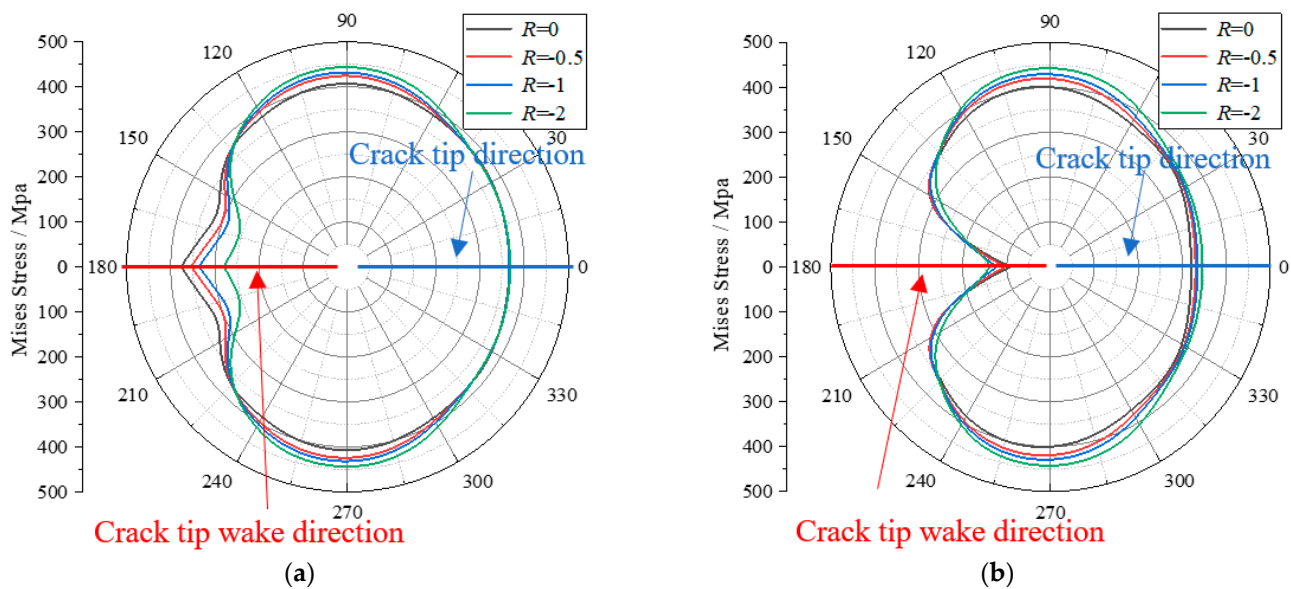


Figure 11. Effect of loading ratio R on Mises stress distribution: (a) Peak loading point, (b) Valley loading point.

The results validate that crack contact closure exists at the crack tip wake zone for specimens under a negative loading ratio again, which will result in different deformation behavior ahead of the crack tip.

4.2.2. Normal Stress Distribution

Normal stress (σ_{yy}) fields during loading processes of $a \sim g$ (in Figure 1) are shown in Figure 12. For specimens under $R = 0$ in Figure 12a,d, normal stresses at peak points a are positive and greater than the yielding stress σ_s , which means that yielding occurs ahead of the crack tip under tensile loading. With loading from peak point a to valley point e , normal stress decreases gradually and then changes to compressive stress, the area of compressive stress is maximum at point e . The area where compressive stress is greater than yielding stress is the reversed plastic area. Normal stress distributions for K3-N and K1-S specimens under $R = 0$ are the same.

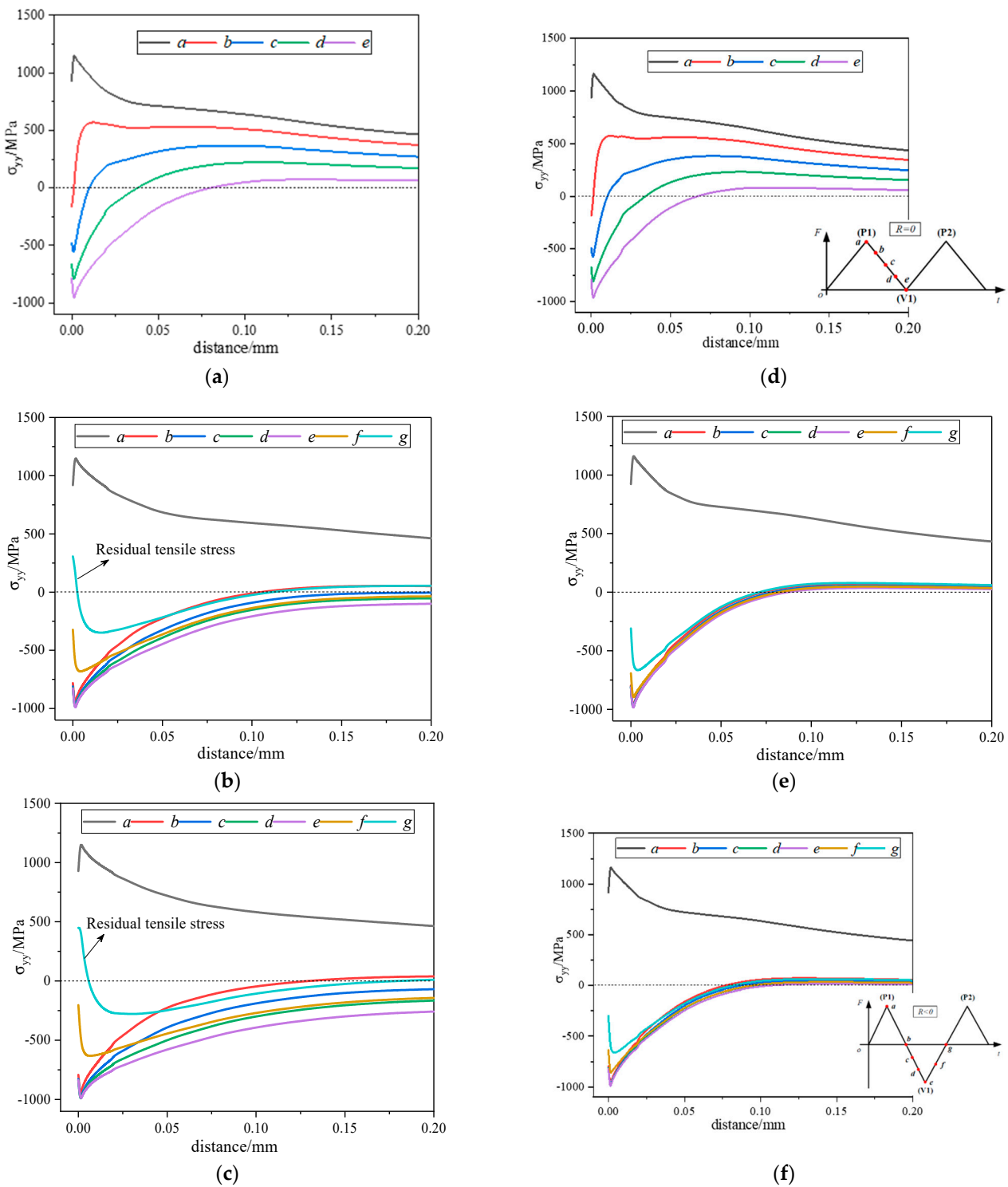


Figure 12. Normal stress distribution of: (a) K3-N, $R = 0$; (b) K3-N, $R = -1$; (c) K3-N, $R = -2$; (d) K1-S, $R = 0$; (e) K1-S, $R = -1$; (f) K1-S, $R = -2$.

For specimens under $R < 0$ in Figure 12b,c,e,f, there are discrepancies of normal stress distributions between different types of specimens, and the differences occur in the stage of $b \sim g$. For the K3-N specimen, as the loading from point b to point e , compressive stress becomes greater, and the area of compressive stress becomes larger too; during loading from point e to point f again, compressive stress becomes smaller; when it is loading to point g , the normal stress in a small range near the crack tip changes to tensile stress again,

with the applied load compressive though. The normal tensile stress at point g is the residual tensile stress, and the area of normal tensile stress is the residual tensile stress area. Moreover, loading ratio R has an obvious effect on the residual tensile stress zone. The smaller the loading ratio R , the larger the residual tensile stress zone and the greater the crack growth driving force, which is consistent with the conclusion in references [18,22].

For the K1-S specimen with $R < 0$, when the load is gradually unloading from point b to point e , compressive stress distribution at the crack tip almost remains unchanged; this is mainly due to the high degree of crack contact closure, which hinders the generation of reverse plastic strain at the crack tip. With the load from point e to point f and then to point g , the compressive stress distribution changes slightly with normal stress still compressive; there is no residual tensile stress zone, and loading ratio R has almost no effect on the stress field.

Therefore, the size of the residual tensile stress zone is not only related to the negative stress ratio but also related to the contact degree; it can be concluded that there is no residual tensile stress zone when contact degree of the specimen is greater enough, while residual tensile stress zone increases with loading ratio decreasing when contact degree of the specimen is smaller enough.

5. Monotonous Plastic Zone, Reversed Plastic Zone and Residual Tensile Plastic Zone

Plastic deformation ahead of the crack tip for specimen under negative fatigue loading ratio is divided into an elastic zone, monotonous plastic zone, reversed plastic zone and residual tensile plastic zone, as shown in Figure 13. When the loading is from 0 to P_{\max} ($0 \sim a$), the outer zone is the linear-elastic zone, where the deformation is mainly elastic. Meanwhile, irreversible plastic deformation occurs within the elastic zone, which is called the Monotonous plastic zone, whose mechanical properties depend on K_{\max} . When the loading is from P_{\max} to P_{\min} ($a \sim e$), the elastic zone gradually recovers, and the reversed plastic deformation occurs due to the squeeze in the inner Monotonous plastic zone. Meanwhile, reversed plastic zone occurs within the Monotonous plastic zone, whose mechanical properties are dependent on ΔK . When the loading is from P_{\min} to P_{\max} again ($e \sim g$), the linear elastic zone expands again, and the Monotonous plastic zone is forced to expand. At this time, even if the compressive load is still applied near the crack tip, a residual tensile plastic zone that can accelerate crack propagation is formed in the monotonic plastic zone, and its internal mechanical behavior depends on R . The residual tensile plastic zone expands continuously with the increase of load until it becomes a monotonic plastic zone at g point, and then the reverse plastic zone formed by unloading will be covered by a monotonic plastic zone.

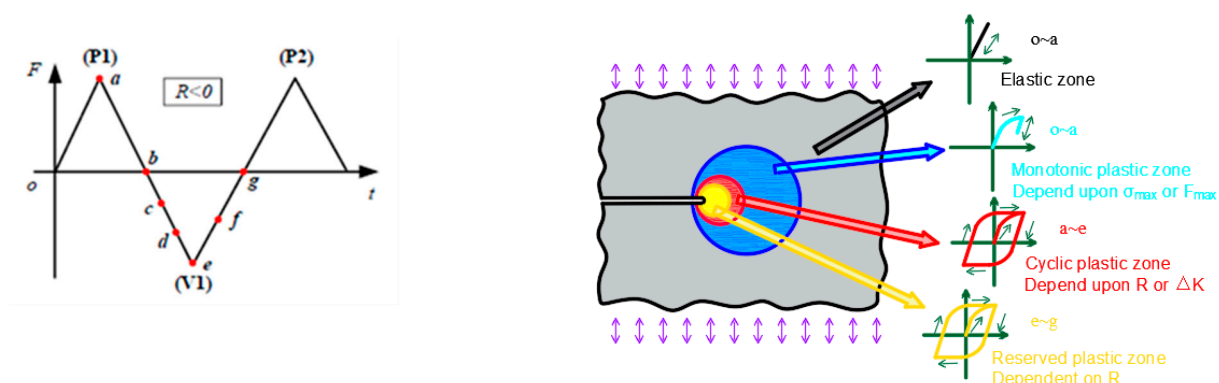


Figure 13. Diagram of various plastic zones of the crack tip [18,21].

The above zones during loading–unloading have close relationships with fatigue crack growth behaviors, so the zones of Monotonous plastic zone, Reversed fatigue zone and Residual tensile plastic zone will be discussed in the following to figure out the effect of constraint, CL effect and contact closure on fatigue crack growth.

The monotonic plastic zone can be defined as the zone where the EPS at crack tip is higher than or equal to 10^{-4} [18]. The reverse plastic zone is the plastic zone generated during the unloading process, which can be judged by whether it is increased during the unloading process of EPS [18]. The residual tensile plastic zone occurs during reloading, which can be judged by the zone where the positive stress is greater than 0. The relationships between Monotonic plastic zones with stress ratio R and specimen type (constraint and contact degree) are shown in Figure 14a, and the relationships between the Reverse plastic zone and Residual tensile plastic zone are shown in Figure 14b,c, respectively.

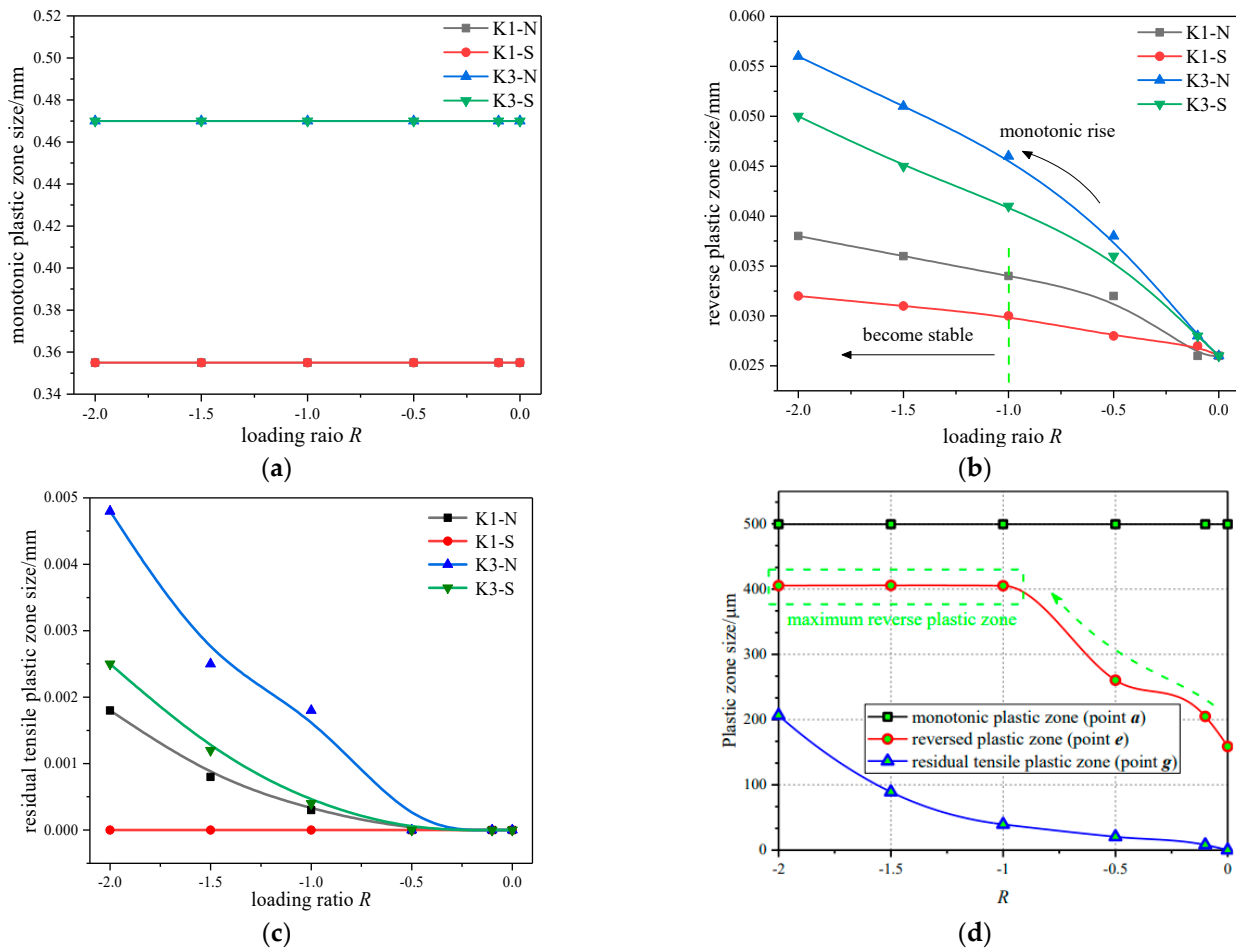


Figure 14. Relationships of plastic zones: (a) Monotonous plastic zone; (b) Reversed plastic zone; (c) Residual tensile plastic zone; (d) Results in the paper [18].

Firstly, the monotonic plastic zone in Figure 14a is related to the crack tip constraint. The higher/lower the constraint B , the smaller/larger the monotonic plastic zone. The CL effect and the contact degree C have no effect on the monotonic plastic zone.

Reversed plastic zone in Figure 14b is related to loading ratio R and contact degree C (CL effect). The main findings are as follows: With the decrease of loading ratio R , the size of Reversed plastic zone increases gradually, but the increasing amplitude is related to the contact degree C (CL effect). The Reversed plastic zone at the crack tip of the K3-N specimen increases fastest with R , and the K1-S specimen has the lowest increasing rate. That is, the greater (smaller) the contact degree C (CL effect), the smaller the increasing rate of the Reversed plastic zone (RPZ) with R . Especially for the K1-S specimen, the size of RPZ almost remains unchanged with $R < -1$. This is mainly because the greater the contact degree C , the greater the crack closure degree, and the smaller the Reversed plastic zone produced by unloading.

The Residual tensile plastic zone (RTPZ) in Figure 14c is also related to loading ratio R and contact degree C (CL effect). With the decrease of loading ratio R , the size of RTPZ increases gradually except for the K1-S specimen, which always keeps zero. From the figure, it can be obtained that the greater (smaller) the contact degree C (CL effect), the larger (smaller) the RTPZ.

Zhang [18] also obtained similar conclusions in the study of crack tip mechanical behaviors of CTS specimens, but the influence of contact degree was not discussed in Zhang's paper, which is shown in Figure 14d. The results of Zhang also can demonstrate the accuracy of the results in this paper.

6. Strain Energy Analyses

6.1. Hysteresis Loop

Figure 15 shows the stress–strain hysteresis loop of the node point 2 μm away from the crack tip at the 10th cycle, where S_{yy} and E_{yy} are normal stress and strain perpendicular to the crack direction and where Figure 15a,b show the effect of loading ratio and effect of specimen type on hysteresis loop.

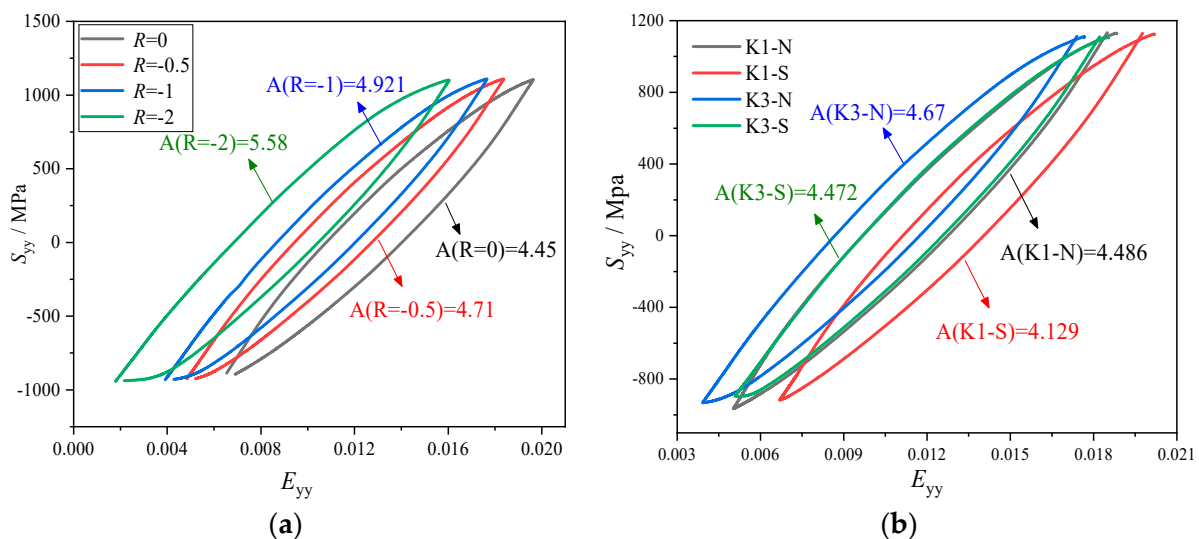


Figure 15. Hysteresis loop: (a) effect of loading ratio R ; (b) effect of specimen type.

Firstly, the hysteresis loop gradually moves to the left as the loading ratio decreases, as shown in Figure 15a. The area enclosed by the hysteresis loop is the strain energy required to drive the crack. The smaller the R , the higher the dissipation energy at the crack tip. Therefore, the negative load can promote damage to the crack tip materials. Then for the effect of specimen type in Figure 15b, the hysteresis loop of the K1-S specimen is at the rightmost, and the K3-N specimen is at the leftmost. The area enclosed by the hysteresis loop of the K3-N specimen is the largest, and the area of the K1-S specimen is the smallest. This is mainly because the ligament of the K3-N specimen bears higher compressive stress, and then the crack tip generates higher energy to drive crack propagation.

Combined with B , CL effect and C in Figure 4, conclusions can be obtained: For specimens under different loading ratios, the smaller the R , the higher the contact degree C and the greater the CL effect, with the CL effect greater than that of C . So the strain energy at the crack tip increases with R decreasing. For different types of specimens under the same loading ratio R , the higher the contact degree C , or the lower the CL effect, the smaller the strain energy, and the less easy it is for the crack to extend.

6.2. Strain Energy Analyses

The evolution of elastic and plastic strain energy at the crack tip is given in Figure 16. In the figure, during the process from unloading to loading, the elastic strain energy under-

goes: decreasing (tensile linear elastic recovery stage)~increasing (reversal compression stage)~decreasing (compressive linear elastic recovery stage)~increasing (forward tensional stage). When it returns to the peak load again, the elastic strain energy returns to the original value, indicating that the elastic strain energy does not play a role in the crack extension. In contrast, the plastic strain energy gradually increases in the loading–unloading process, which indicates that the plastic strain energy gradually accumulates in the process. During the process, the plastic strain energy first remains constant (tensile linear elastic recovery stage) and then increases (plastic accumulation stage). When the load is loaded again, plastic strain energy first remains constant (compressive linear elastic recovery stage) until the crack surface separates and the tensile load to the crack tip produces plastic deformation (plastic accumulation stage).

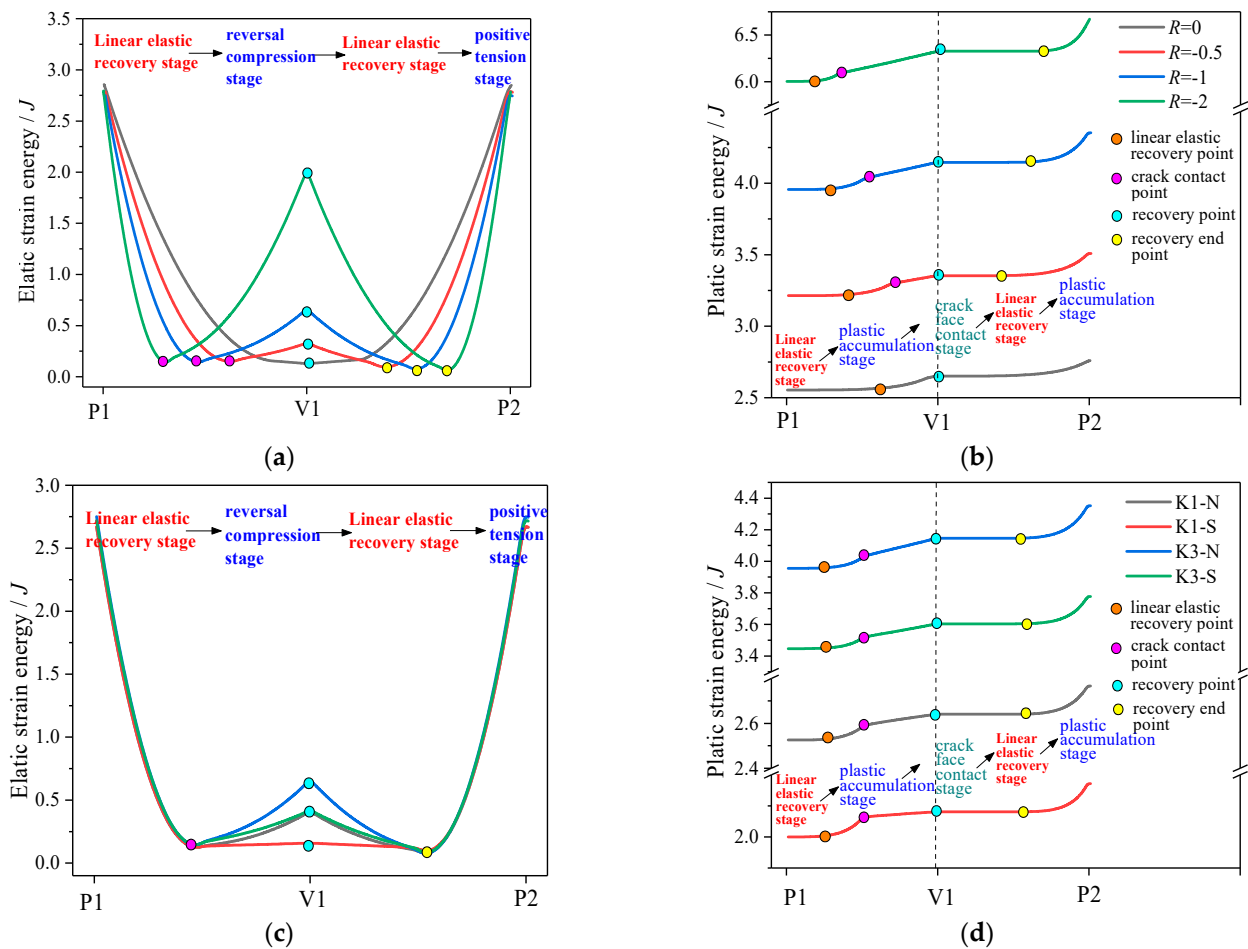


Figure 16. Elastic and Plastic strain energy: (a) effect of R on elastic strain energy; (b) effect of R on plastic strain energy; (c) effect of specimen type on elastic strain energy; (d) effect of specimen type on plastic strain energy.

The whole process of strain energy is consistent with that of EPS in Figures 9 and 10, which is also related to the CL effect and contact degree C .

7. EPS Field Analyses for I–II Mixed Mode Crack (without Considering Shear Friction)

The effects of constraint B , CL effect and contact degree C on mode I crack tip fields were studied in the above paper. For I–II mixed crack, the crack tip can be decomposed to mode I and mode II components, of which mode I crack is also influenced by constraint, CL effect and contact degree, and the law is consistent with the above. In contrast, mode II crack does not have any constraint effect and crack contact closure due to shear deformation (without considering shear friction), so only the negative loading ratio effect needs to be

considered. In the following, the relationship between the mechanical behavior at the crack tip and the loading ratio for I-II mixed mode crack will be briefly discussed through the EPS field of the K3-N specimen.

The EPS distributions at crack tips of pure mode II cracks acting at loading angles of $\beta = 0^\circ$ and I-II mixed mode cracks acting at $\beta = 60^\circ$ are given in Figure 17. From the figure, it can be found that plastic strain accumulation at the pure mode II crack tip is much greater than that at I-II mixed crack tip. Moreover, for the mode II crack in Figure 17a, EPS under $R = -1$ is approximately 3.4 times that under $R = 0$, and EPS under $R = -2$ is approximately 2.5 times that under $R = -1$. In contrast, for the I-II mixed mode crack in Figure 17b, EPS under $R = -1$ is only approximately 2.2 times that under $R = 0$ and EPS under $R = -2$ is only 1.4 times that under $R = -1$.

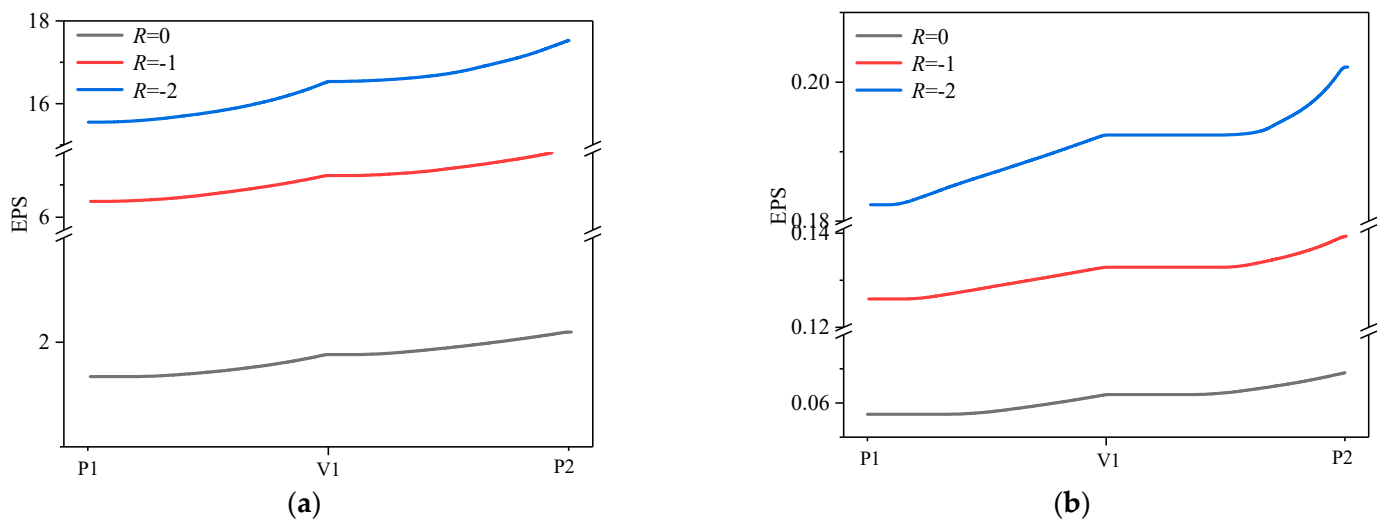


Figure 17. EPS field with loading history: (a) $\beta = 0^\circ$, (b) $\beta = 60^\circ$.

In addition, for pure mode II crack, the increasing process of EPS with loading history is less affected by loading ratio R (shown in Figure 17a). In contrast, for I-II mixed mode crack under $\beta = 60^\circ$, the increasing law of EPS with the loading history is much more influenced by loading ratio R (shown in Figure 17b), which is similar to that of mode I crack in Figure 9.

It is mainly due to the fact that there is no crack contact closure in the mode II crack, while there is contact closure of the mode I component in the I-II mixed mode crack, which hinders plastic strain accumulation at the crack tip to a certain degree.

The circular distribution of EPS is given in Figure 18. The EPS field of mode II and I-II mixed mode crack tip shows a symmetrical shape. For pure mode II crack under $\beta = 0^\circ$, the EPS of the specimen under $R = -2$ is much greater than that under $R = 0$ in Figure 18a. Meanwhile, for I-II mixed mode crack, the difference in EPS between the two loading ratios in Figure 18b is smaller. It is considered that there exists no crack contact closure effect during the mode II fatigue loading–unloading process. Moreover, for I-II mixed mode crack, crack closure will be induced by the mode I component, which prevents the plastic strain accumulation at the crack tip. So, the crack contact effect can be ignored for specimens under negative loading ratios when the mode II component is dominant.

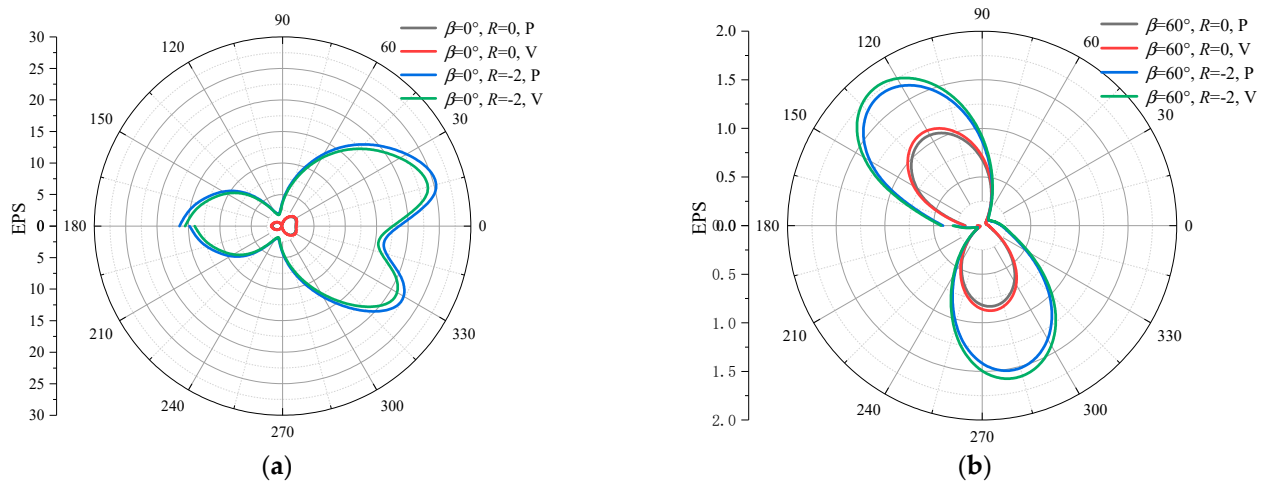


Figure 18. Circumferential EPS field: (a) $\beta = 0^\circ$, (b) $\beta = 60^\circ$.

8. Conclusions

This paper focuses on the study of mechanical behaviors at the crack tip of specimens under negative loading ratios by the finite element method. Three factors, including constraint, CL effect and contact degree are mainly discussed. The main conclusions are obtained as follows:

(1) The factors of constraint, CL effect and contact degree have many effects on the fatigue stress–strain field. For plastic strain field with $R \geq 0$, the constraint effect is the main factor, CL effect and contact degree have no effect. Meanwhile, for a plastic strain field with $R < 0$, the greater the CL effect, the lower the contact degree and the greater the plastic strain accumulation ahead of the crack tip. For stress fields with $R < 0$, no residual tensile stress zone with a contact degree is greater enough, while the residual tensile stress zone increases with the loading ratio decreasing with a contact degree smaller enough.

(2) Three zones of Monotonic plastic zone, Reverse plastic zone (RPZ) and Residual tensile plastic zone (RTPZ) ahead of crack tips are related to the CL effect and contact degree. The higher/lower the constraint B , the smaller/larger the monotonic plastic zone. The greater (smaller) the contact degree C (CL effect), the smaller the increase rate of the Reverse plastic zone (RPZ) with R , which is mainly because the greater the contact degree C , the greater the crack closure degree and the smaller the RPZ produced by unloading. RTPZ is also related to loading ratio R and contact degree C (CL effect). The greater (smaller) the contact degree C (CL effect), the smaller the RTPZ.

(3) There is no constraint effect and crack contact closure for mode II fatigue crack due to shear deformation; only the negative loading ratio effect needs to be considered. Plastic strain accumulation ahead of the crack tip of the mode II crack is greater than that of the mode I crack; due to this, there is no crack contact closure effect in the mode II crack. For the I-II mixed crack, the crack tip can be decomposed to the mode I and mode II components, of which the mode I crack is also influenced by constraint, CL effect and contact degree, and the law is consistent with the above conclusion.

Author Contributions: Conceptualization, X.M. and H.H.; methodology, X.M.; software, X.H. and H.H.; validation, J.P.; investigation, X.M.; writing—original draft preparation, X.H.; writing—review and editing, X.H. and H.H.; supervision, F.B.; funding acquisition, X.M. and J.P. All authors have read and agreed to the published version of the manuscript.

Funding: This research was funded by National Natural Science Foundation of China [52105141, 52075050], Natural Science Research of Jiangsu Higher Education Institutions of China [21KJB460002], Natural Science Foundation of Jiangsu Province [BK20201448], Science and Technology project of Changzhou [CJ20200080].

Institutional Review Board Statement: Not applicable.

Informed Consent Statement: Not applicable.

Data Availability Statement: Not applicable.

Conflicts of Interest: The authors declare no conflict of interest.

References

1. Zhang, J.; He, X.D.; Sha, Y.; Du, S.Y. The compressive stress effect on fatigue crack growth under tension–compression loading. *Int. J. Fatigue* **2010**, *32*, 361–367. [[CrossRef](#)]
2. Rozylo, P.; Falkowicz, K. Stability and failure analysis of compressed thin-walled composite structures with central cut-out, using three advanced independent damage models. *Compos. Struct.* **2021**, *273*, 114298. [[CrossRef](#)]
3. Zhang, P.; Zhou, C.Y.; Xie, L.Q.; He, X.H. Numerical investigation of mechanical behavior of crack tip under mode I and mixed-mode I-II fatigue loading at negative load ratios. *Theor. Appl. Fract. Mech.* **2020**, *108*, 102673. [[CrossRef](#)]
4. Miao, X.; Jiang, C.Y.; Zhou, C.Y.; Peng, J.; Gao, G. Effects of specimen type and thickness on elastic and elastic–plastic fracture parameters for I-II and I-III mixed mode cracks. *Theor. Appl. Fract. Mech.* **2021**, *115*, 103042. [[CrossRef](#)]
5. Larsson, S.G.; Carlsson, A.J. Influence of non-singular stress terms and specimen Geometry on small-scale yielding at crack tips in elastic-plastic materials. *J. Mech. Phys. Solids* **1973**, *21*, 263–277. [[CrossRef](#)]
6. Varfolomeev, I.; Luke, M.; Burdack, M. Effect of specimen geometry on fatigue crack growth rates for the railway axle material EA4T. *Eng. Fract. Mech.* **2011**, *78*, 742–753. [[CrossRef](#)]
7. Hutar, P.; Seitzl, S.; Knésl, Z. Effect of constraint on fatigue crack propagation near threshold in medium carbon steel. *Comput. Mater. Sci.* **2006**, *37*, 51–57. [[CrossRef](#)]
8. Ayatollahi, M.R.; Rashidi Moghaddam, M.; Berto, F. T-stress effects on fatigue crack growth-theory and experiment. *Eng. Fract. Mech.* **2018**, *187*, 103–114. [[CrossRef](#)]
9. Tong, J. T-stress and its implications for crack growth. *Eng. Fract. Mech.* **2002**, *69*, 1325–1337. [[CrossRef](#)]
10. Zhao, J.H.; Guo, W.L.; She, C.M. The in-plane and out-of-plane stress constraint factors and K-T-Tz description of stress field near the border of a semi-elliptical surfaces crack. *Int. J. Fatigue* **2007**, *29*, 435–443. [[CrossRef](#)]
11. Xu, L. Three-Dimensional Fatigue Crack Growth Analyses Based on Crack Closure Mode. Ph.D. Thesis, Nanjing University of Aeronautics and Astronautics, Nanjing, China, 2018. (In Chinese).
12. Liknes, H.O.; Stephens, R.R. Effect of geometry and load history on fatigue crack growth in Ti-62222. *ASTM Spec. Tech. Publ.* **2000**, *1372*, 175–191.
13. Deka, N.; Jonnalagadda, K.N. Effect of Constraint and Latent Hardening ratio on the Plastic Flow around a Crack Tip in a Hardening FCC Single Crystal. *Int. J. Plast.* **2018**, *115*, 132–153. [[CrossRef](#)]
14. *ASTM E647-15*; Test Method for Measurement of Fatigue Crack Growth Rates. ASTM International: West Conshohocken, PA, USA, 2015; Volume 3, pp. 647–695.
15. Huang, X.; Wang, A.; Cui, W. The Fatigue Crack Growth under Compressive to Compressive Fluctuating Loading. In Proceedings of the ASME, International Conference on Offshore Mechanics and Arctic Engineering, 29th International Conference on Ocean, Offshore and Arctic Engineering, Shanghai, China, 21–30 July 2010.
16. Pommier, S.; Bompard, P. Bauschinger effect of alloys and plasticity induced crack closure: A finite element analysis. *Fatigue Fract. Eng. Mater. Struct.* **2000**, *23*, 129–139. [[CrossRef](#)]
17. Bian, R.G.; Cui, W.C.; Wan, Z.Q. Study on crack propagation under compressive-compressive fatigue based on two parameter unified method. *Ship Mech.* **2009**, *5*, 734–738. (In Chinese)
18. Zhang, P.; Zhou, C.Y.; Li, J.; Miao, X.T.; He, X.H. Effect of compressive load and crack closure on fatigue crack growth of commercial pure titanium at negative load ratios. *Eng. Fract. Mech.* **2019**, *219*, 106622. [[CrossRef](#)]
19. *GB/T 6398-2017*; Metallic Materials—Fatigue Testing—Fatigue Crack Growth Method. China Standards Press: Beijing, China, 2017. (In Chinese)
20. Ivanytskyj, Y.L.; Lenkovskiy, T.M.; Molkov, Y.V.; Kulyk, V.V.; Duriagina, Z.A. Influence of 65G steel microstructure on crack faces friction factor under mode II fatigue fracture. *Arch. Mater. Sci. Eng.* **2016**, *82*, 49–56. [[CrossRef](#)]
21. Zhang, P.; Xie, L.Q.; Zhou, C.Y.; He, X.H. Experimental and numerical investigation on fatigue crack growth behavior of commercial pure titanium under I-II mixed mode loading at negative load ratios. *Int. J. Fatigue* **2020**, *138*, 105700. [[CrossRef](#)]
22. Chaboche, J.L. Time-independent constitutive theories for cyclic plasticity. *Int. J. Plast.* **1986**, *2*, 149–188. [[CrossRef](#)]
23. Ostash, O.P.; Panasyuk, V.V.; Andreiko, I.M. Methods for the construction of the diagrams of fatigue crack-growth rate of materials. *Mater. Sci.* **2007**, *43*, 479–491. [[CrossRef](#)]
24. Miao, X.T.; Zhou, C.Y.; Lv, F.; He, X.H. Three-dimensional finite element analyses of T-stress for different experimental specimens. *Theor. Appl. Fract. Mech.* **2017**, *91*, 116–125. [[CrossRef](#)]